Tensor Algebra and Multidimensional Harmonic Retrieval in Signal Processing for MIMO Radar

Dimitri Nion and Nicholas D. Sidiropoulos, *Fellow, IEEE*

***Abstract*—Detection and estimation problems in multiple-input multiple-output (MIMO) radar have recently drawn considerable interest in the signal processing community. Radar has long been a staple of signal processing, and MIMO radar presents challenges and opportunities in adapting classical radar imaging tools and developing new ones. Our aim in this article is to showcase the potential of tensor algebra and multidimensional harmonic retrieval (HR) in signal processing for MIMO radar. Tensor algebra and multidimensional HR are relatively mature topics, albeit still on the fringes of signal processing research. We show they are in fact central for target localization in a variety of pertinent MIMO radar scenarios. Tensor algebra naturally comes into play when the coherent processing interval comprises multiple pulses, or multiple transmit and receive subarrays are used (multistatic configuration). Multidimensional harmonic structure emerges for far-field uniform linear transmit/receive array configurations, also taking into account Doppler shift; and hybrid models arise in-between. This viewpoint opens the door for the application and further development of powerful algorithms and identifiability results for MIMO radar. Compared to the classical radar-imaging-based methods such as Capon or MUSIC, these algebraic techniques yield improved performance, especially for closely spaced targets, at modest complexity.**

***Index Terms*—DoA-DoD estimation, harmonic retrieval, localization, multiple-input multiple-output (MIMO) radar, tensor decomposition.**

I. Introduction

RECENTLY, the concept of multiple-input multiple-output (MIMO) radar has drawn considerable attention (see [2], [3], and references therein). A MIMO radar utilizes multiple antennas at both the transmitter and the receiver end, but unlike conventional phased-array radar, it can transmit linearly independent waveforms. This waveform diversity endows MIMO radar with superior capabilities relative to phased-array radar. One can distinguish two main classes of MIMO radar, employing widely separated [3] or co-located antennas [2], respectively. The first class capitalizes on the rich scattering properties of a target by transmitting linearly independent signals from sufficiently spaced antennas that illuminate the target from ideally decorrelated aspects. The second class allows to model a target as a point-source in the far field and uses MIMO spatial signatures to estimate the parameters of interest via coherent processing.

In this paper, we focus on the problem of estimating the localization parameters of multiple targets in a given range bin via coherent processing techniques. The parameters of interest include direction of arrival (DoA), direction of departure (DoD), and Doppler shift; but also a target's spatial signature or radar cross section (RCS). We will consider the following three MIMO radar configurations.

- **Configuration 1: Single-pulse, bistatic case**. In this configuration, the targets are illuminated by an array of M closely spaced antennas and the reflected waveforms are received by an array of N closely spaced antennas. The transmit and receive arrays are not necessarily colocated (bistatic case). The propagation environment is assumed to be nondispersive. The coherent processing interval (CPI) consists of a single pulse period.
- **Configuration 2: Multiple-pulses, bistatic case**. In this scenario, the spatial configuration is the same as in the first configuration but the CPI now consists of Q consecutive pulse periods. We distinguish between the Swerling I target model, where the RCS of all targets is constant during the CPI, and the Swerling II target model, where it is varying from pulse to pulse. In both cases, we assume that the medium is nondispersive.
- **Configuration 3: Multiple-pulses, multistatic case**. In this configuration, the transmitter is equipped with $\tilde{M}$ nonoverlapping subarrays and the receiver with $\tilde{N}$ nonoverlapping subarrays. Each transmit and receive subarray consists of closely spaced antennas, while the subarrays are sufficiently spaced to ensure that they experience independent RCS fading coefficients. As in the previous configurations, the targets are located in the far-field. The RCS coefficients are assumed to vary independently from pulse to pulse (Swerling II), and the propagation medium is nondispersive.

DoA/DoD estimation in MIMO radar can be accomplished using 1-D or 2-D radar-imaging techniques [2], [4]–[8], which look for peaks in a beamformer output spectrum, computed for every angle (or pair of angles in the bistatic case) in a region of interest. The main issues with these techniques are the following:

i) **Limited spatial resolution:** detection and localization typically fail for closely spaced targets, since a single lobe may then occur in the output spectrum;
ii) **Sensitivity to fading:** changing a target aspect by as little as one milliradian may result in variations of the reflected

Manuscript received April 20, 2010; accepted July 05, 2010. Date of publication July 15, 2010; date of current version October 13, 2010. The associate editor coordinating the review of this manuscript and approving it for publication was Dr. Kainam Thomas Wong. The work of D. Nion was supported by the French Délégation Générale pour l'Armement (DGA) by a Postdoctoral Grant. The material in this paper was presented in part at the IEEE International Conference on Acoustics, Speech, and Signal Processing (ICASSP) 2009.

D. Nion is with Group Science, Engineering and Technology, K.U. Leuven, Campus Kortrijk, Belgium (e-mail: Dimitri.Nion@kuleuven-kortrijk.be).

N. D. Sidiropoulos is with the Department of ECE, Technical University of Crete, 73100 Chania, Greece (e-mail: nikos@telecom.tuc.gr).

Color versions of one or more of the figures in this paper are available online at http://ieeexplore.ieee.org.

Digital Object Identifier 10.1109/TSP.2010.2058802

power of 20 dB or more. Application of radar-imaging on a per-pulse basis thus gives rise to a target scintillation phenomenon; and

iii) **High complexity:** the final image is generated after angular scanning, which may become highly time-consuming for a dense angular grid, especially in the 2-D case.

A growing number of applications involve signals that are naturally represented as N-D arrays, or Nth-order tensors, rather than 2-D arrays, i.e., matrices. Signal processing tools based on multilinear tensor algebra allow us to exploit the strong algebraic structure of these multidimensional signals; we refer to [9], [10], and references therein for a review of these tools. PARAllel FACtor (PARAFAC) analysis [11], [12] decomposes a tensor in a sum of rank-one tensors. A rank-one tensor of order N is an outer product of N *loading* vectors. The rank of a tensor is the smallest number of rank-one tensors needed to synthesize the given tensor as their sum. PARAFAC is thus tied to the concept of tensor rank and low-rank decomposition. In this sense, PARAFAC is one possible generalization of the matrix singular value decomposition (SVD) to the higher-order case. PARAFAC exhibits strong uniqueness properties without imposing orthogonality of the loading vectors [13]–[15]. In practice, however, it is often desirable to impose application—specific constraints on the loadings of the PARAFAC decomposition. In applications in Chemometrics, for instance, nonnegativity constraints are often meaningful [16]. In sensor array processing, one or more loading matrices of the PARAFAC decomposition may have strong algebraic structure [17], e.g., Vandermonde. In the 2-D case, a matrix factorization problem of the form $\mathbf{Y} = \mathbf{A}\mathbf{B}^T$ where the unknown matrix factors $\mathbf{A}$ and $\mathbf{B}$ both have Vandermonde structure is a 2-D harmonic retrieval (2-D HR) problem. By extension, the PARAFAC decomposition of an Nth-order tensor in which all loading matrices have a Vandermonde structure is an N-D harmonic retrieval problem. Several algorithms and uniqueness results have been derived for 2-D and N-D HR problems; see, e.g., [18]–[25], and references therein. Pertinent applications of PARAFAC and N-D HR to MIMO channel sounding problems have been considered in [26] and [27].

In this paper, we revisit the MIMO radar data models considered in [4]–[8], [28], and show that, for the three configurations previously listed, detection and localization of multiple targets can be achieved via appropriate tensor decompositions and multidimensional harmonic retrieval tools. These techniques offer the following advantages relative to spectral-Capon and spectral-MUSIC radar imaging methods considered in the aforementioned references:

i) **Improved identifiability and spatial resolution:** it is possible to localize closely spaced targets with relatively good accuracy. Owing to a well-developed identifiability theory, it is also possible to pin down fundamental limits on the number of resolvable point scatterers.

ii) **Robustness to fading:** the RCS fluctuations from pulse to pulse (in the case of a Swerling II target model) are not regarded as a nuisance, but rather as a source of diversity.

iii) **Simplicity:** the DoAs and DoDs are obtained from a single algebraic decomposition (including automatic pairing), without need for angular scanning and peak detection.

Preliminary results on applications of PARAFAC to MIMO radar have appeared in conference form in [1]. This journal version adds multidimensional harmonic decomposition tools, considers three different radar configurations, establishes a link between the multistatic case and a generalization of PARAFAC known as block component decomposition (BCD), and includes extensive experiments.

The rest of this paper is organized as follows. Some multilinear algebra prerequisites are introduced in Section II. In Section III, we focus on the first configuration and establish a link to the 2-D HR problem when a uniform linear array (ULA) geometry is assumed at the transmitter and the receiver. In Section IV, we show that, for the second configuration, the localization problem amounts to the computation of a PARAFAC decomposition for general array geometries, and a multidimensional HR problem for ULA geometries. In Section IV, we show that the data model for the third configuration can be regarded as a tensor decomposition in block-terms. Section VI reports numerical results and Section VII summarizes our conclusions.

Notation: A third-order tensor of size $I \times J \times K$ is denoted by a calligraphic letter $\mathcal{Y}$, and its elements are denoted by y_{ijk}, $i = 1, \ldots, I$, $j = 1, \ldots, J$ and $k = 1, \ldots, K$. $\mathbf{Y}$ denotes a matrix and $\mathbf{y}$ a vector. The transpose, complex conjugate, complex conjugate transpose, and pseudoinverse are denoted by $\mathbf{Y}^T$, $\mathbf{Y}^*$, $\mathbf{Y}^H$, and $\mathbf{Y}^\dagger$, respectively. $||\mathbf{Y}||_F$ denotes the Frobenius norm. $\mathrm{vec}(\mathbf{Y})$ is the operator that stacks the columns of $\mathbf{Y}$ one after each other in a single vector. $\mathrm{diag}(\mathbf{y})$ is a diagonal matrix that holds the entries of $\mathbf{y}$ on its diagonal. $\mathrm{Diag}(\mathbf{A}_1, \mathbf{A}_2, \ldots, \mathbf{A}_M)$ is a block-diagonal matrix with $\mathbf{A}_1, \mathbf{A}_2, \ldots, \mathbf{A}_M$ being its diagonal submatrices. The Kronecker product is denoted by $\otimes$. The Khatri-Rao product (or column-wise Kronecker product) is denoted by $\odot$, i.e., $[\mathbf{a}_1, \ldots, \mathbf{a}_I] \odot [\mathbf{b}_1, \ldots, \mathbf{b}_I] = [\mathbf{a}_1 \otimes \mathbf{b}_1, \ldots, \mathbf{a}_I \otimes \mathbf{b}_I]$. The $P \times P$ identity matrix is denoted by $\mathbf{I}_P$. We will also use a Matlab-type notation for matrix subblocks, i.e., $[\mathbf{A}]_{l:m,n:p}$ represents the matrix built after selection of $m - l + 1$ rows of $\mathbf{A}$, from the lth to the mth, and $p - n + 1$ columns of $\mathbf{A}$, from the nth to the pth. $[\mathbf{A}]_{:,n:p}$ is used to denote selection of all rows and $[\mathbf{A}]_{l:m,:}$ to denote selection of all columns. The column-wise concatenation of two matrices $\mathbf{A}$ and $\mathbf{B}$ having the same number of rows is denoted by $[\mathbf{A},\ \mathbf{B}]$. The ceiling operator is denoted by $\lceil \cdot \rceil$.

II. Multilinear Algebra Prerequisites

Definition 1 (Matrix Unfoldings): The three standard matrix unfoldings of a third-order tensor $\mathcal{X} \in \mathbb{C}^{I \times J \times K}$, denoted by $\mathbf{X}^{(1)} \in \mathbb{C}^{IK \times J}$, $\mathbf{X}^{(2)} \in \mathbb{C}^{JI \times K}$, and $\mathbf{X}^{(3)} \in \mathbb{C}^{KJ \times I}$ are defined by $[\mathbf{X}^{(1)}]_{(i-1)K+k,j} = x_{ijk}$, $[\mathbf{X}^{(2)}]_{(j-1)I+i,k} = x_{ijk}$ and $[\mathbf{X}^{(3)}]_{(k-1)J+j,i} = x_{ijk}$, respectively.

Definition 2 (Mode-n Tensor-Matrix Product): The mode-1 product of $\mathcal{Y} \in \mathbb{C}^{L \times M \times N}$ by a matrix $\mathbf{A} \in \mathbb{C}^{I \times L}$, denoted by $\mathcal{Y} \bullet_1 \mathbf{A}$, is an $(I \times M \times N)$-tensor with elements defined, for all index values, by $(\mathcal{Y} \bullet_1 \mathbf{A})_{imn} = \sum_{l=1}^{L} y_{lmn} a_{il}$. Similarly, the mode-2 product by a matrix $\mathbf{B} \in \mathbb{C}^{J \times M}$ and the mode-3 product by $\mathbf{C} \in \mathbb{C}^{K \times N}$ are the $(L \times J \times N)$ and $(L \times M \times K)$

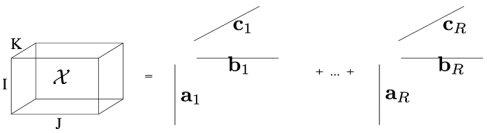

Fig. 1. Schematic representation of PARAFAC decomposition.

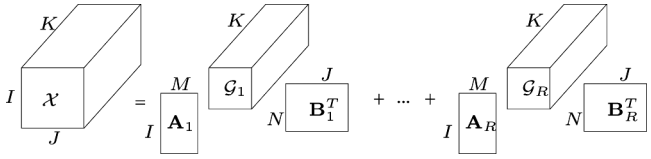

Fig. 2. Schematic representation of the BCD-$(M,\ N, \cdot)$ of $\mathcal{X}$.

tensors, respectively, with elements defined by $(\mathcal{Y} \bullet_2 \mathbf{B})_{ljn} = \sum_{m=1}^{M} y_{lmn} b_{jm}$ and $(\mathcal{Y} \bullet_3 \mathbf{C})_{lmk} = \sum_{n=1}^{N} y_{lmn} c_{kn}$.

Definition 3 (PARAFAC in Element-Wise Format): The parallel factor decomposition [11] of a third-order tensor $\mathcal{X} \in \mathbb{C}^{I \times J \times K}$ in R factors, represented in Fig. 1, is a decomposition of the form

$$x_{ijk} = \sum_{r=1}^{R} a_{ir} b_{jr} c_{kr} \Longleftrightarrow \mathcal{X} = \sum_{r=1}^{R} \mathbf{a}_r \circ \mathbf{b}_r \circ \mathbf{c}_r \qquad (1)$$

where the $I \times R$, $J \times R$, and $K \times R$ matrices $\mathbf{A}, \mathbf{B}$, and $\mathbf{C}$ defined by $[\mathbf{A}]_{i,r} = a_{ir}$, $[\mathbf{B}]_{j,r} = b_{jr}$, $[\mathbf{C}]_{k,r} = c_{kr}$, respectively, are the so-called "loading matrices" of the decomposition, $\mathbf{a}_r$, $\mathbf{b}_r$, and $\mathbf{c}_r$ denote the rth column of $\mathbf{A}$, $\mathbf{B}$, and $\mathbf{C}$, respectively, and $\circ$ denotes the outer product.

Definition 4 (PARAFAC in Matrix Format): The three matrix unfoldings of a tensor $\mathcal{X} \in \mathbb{C}^{I \times J \times K}$, that follows the PARAFAC decomposition (1), are linked to the loading matrices $\mathbf{A}$, $\mathbf{B}$, and $\mathbf{C}$ as follows: $\mathbf{X}^{(1)} = (\mathbf{A} \odot \mathbf{C})\mathbf{B}^T$, $\mathbf{X}^{(2)} = (\mathbf{B} \odot \mathbf{A})\mathbf{C}^T$, and $\mathbf{X}^{(3)} = (\mathbf{C} \odot \mathbf{B})\mathbf{A}^T$.

Definition 5 (Essential Uniqueness of PARAFAC): The PARAFAC decomposition of $\mathcal{X}$ is said to be *essentially unique* if any matrix triplet $(\tilde{\mathbf{A}},\ \tilde{\mathbf{B}},\ \tilde{\mathbf{C}})$ that also fits the model is related to $(\mathbf{A},\ \mathbf{B},\ \mathbf{C})$ via $\mathbf{A} = \tilde{\mathbf{A}}\mathbf{\Pi}\mathbf{\Lambda}_1$, $\mathbf{B} = \tilde{\mathbf{B}}\mathbf{\Pi}\mathbf{\Lambda}_2$, $\mathbf{C} = \tilde{\mathbf{C}}\mathbf{\Pi}\mathbf{\Lambda}_3$, with $\mathbf{\Lambda}_1$, $\mathbf{\Lambda}_2$, $\mathbf{\Lambda}_3$ arbitrary diagonal matrices satisfying $\mathbf{\Lambda}_1\mathbf{\Lambda}_2\mathbf{\Lambda}_3 = \mathbf{I}_R$ and $\mathbf{\Pi}$ an arbitrary permutation matrix. Conditions for which essential uniqueness is guaranteed have been derived in [13]–[15].

Definition 6 (Harmonic Retrieval): A decomposition of $\mathcal{X} \in \mathbb{C}^{M \times N \times P}$ of the form

$$x_{mnp} = \sum_{r=1}^{R} c_r e^{j(m-1)\mu_r} e^{j(n-1)\psi_r} e^{j(p-1)\gamma_r}$$

is known as a 3-D HR problem. It can be seen a particular case of the PARAFAC decomposition, where the three loading matrices have a Vandermonde structure. A decomposition of $\mathcal{X} \in \mathbb{C}^{M \times N \times P}$ of the form

$$x_{mnp} = \sum_{r=1}^{R} c_{pr} e^{j(m-1)\mu_r} e^{j(n-1)\psi_r}$$

is known as a multiple-snapshots 2-D HR problem. It can be seen as a particular case of the PARAFAC decomposition, where two loading matrices have a Vandermonde structure whereas the third loading matrix has no specific structure.

Recently, a new class of tensor decompositions has been introduced, the so-called Decompositions in Block Terms, also referred to as block-component-decompositions (BCD) [29]–[31]. In this paper, we will need the BCD in rank-$(M,\ N, \cdot)$ terms, compactly written as BCD-$(M,\ N, \cdot)$.

Definition 7 (BCD in Rank-$(m,\ n, \cdot)$ Terms): The BCD-$(M,\ N, \cdot)$ of a third-order tensor $\mathcal{X} \in \mathbb{C}^{I \times J \times K}$, represented in Fig. 2, is a decomposition of $\mathcal{X}$ of the form

$$\mathcal{X} = \sum_{r=1}^{R} \mathcal{G}_r \bullet_1 \mathbf{A}_r \bullet_2 \mathbf{B}_r \qquad (2)$$

in which the $MK \times N$ and $KN \times M$ matrix representations of $\mathcal{G}_r \in \mathbb{C}^{M \times N \times K}$ are full column rank, and $\mathbf{A}_r \in \mathbb{C}^{I \times M}$ (with $I \geq M$) and $\mathbf{B}_r \in \mathbb{C}^{J \times N}$ (with $J \geq N$) are full column rank $r = 1, \ldots, R$ [30].

III. Single-Pulse, Bistatic Configuration

In this section, we establish a link between the data model of the first MIMO radar configuration and the single-snapshot 2-D HR problem.

A. Data Model

Let us consider a MIMO radar system with the following parameters:

- transmit array of M co-located antennas, $m = 1, \ldots, M$;
- receive array of N co-located antennas, $n = 1, \ldots, N$;
- the transmit and receive arrays are not necessarily co-located (bistatic configuration);
- K targets in a range-bin of interest $k = 1, \ldots, K$;
- $\mathbf{S} = [\mathbf{s}_1, \mathbf{s}_2, \ldots, \mathbf{s}_M]^T \in \mathbb{C}^{M \times L}$ holds the M narrowband transmitted pulse waveforms, L being the number of samples per pulse period;
- $\{\beta_k\}_{k=1}^{K}$ are the RCS fading coefficients;
- $\{\theta_k\}_{k=1}^{K}$, $\{\phi_k\}_{k=1}^{K}$ are the DoDs and DoAs with respect to the transmit and receive array normal, respectively,
- $\mathbf{A} = [\mathbf{a}(\theta_1), \ldots, \mathbf{a}(\theta_K)]$ is the $M \times K$ transmit steering matrix and $\mathbf{B} = [\mathbf{b}(\phi_1), \ldots, \mathbf{b}(\phi_K)]$ the $N \times K$ receive steering matrix.

In this section, we consider the radar return for a *single* pulse. A target is modeled as a point-scatterer in the far-field, as commonly assumed in conventional radar systems and in MIMO radar systems with co-located antennas [2]. The baseband received signal at the output of the receive array can be written, after synchronization, as [2], [6], [28], [32]

$$\mathbf{X} = \mathbf{B}\mathbf{\Sigma}\mathbf{A}^T\mathbf{S} + \mathbf{W} \qquad (3)$$

where $\mathbf{X} \in \mathbb{C}^{N \times L}$ collects the samples received by the N antennas, $\mathbf{\Sigma} = \mathrm{diag}(\mathbf{c})$, $\mathbf{c} = [\beta_1, \ldots, \beta_K]$, and $\mathbf{W} \in \mathbb{C}^{N \times L}$ is the residual noise term. Note that, in theory, a clutter term should be

added to (3). In the following, we suppose that the clutter contribution has been filtered from the data in a preprocessing stage via MIMO radar space-time-adaptive-processing (STAP) techniques [28], [32], and that only residual noise (typically modeled as additive white Gaussian—AWGN) remains in the observed data.[1]

Unlike conventional phased-array radars, a MIMO radar can transmit mutually orthogonal waveforms. Assume that $(1/L)\mathbf{S}\mathbf{S}^H = \mathbf{I}_M$. After right multiplication of (3) by $(1/L)\mathbf{S}^H$, the matched-filter output is

$$\mathbf{Y} = \mathbf{B}\mathbf{\Sigma}\mathbf{A}^T + \mathbf{Z} \tag{4}$$

where $\mathbf{Y} = (1/L)\mathbf{X}\mathbf{S}^H \in \mathbb{C}^{N\times M}$ and $\mathbf{Z} = (1/L)\mathbf{W}\mathbf{S}^H$. Vectorization of (4) yields

$$\tilde{\mathbf{y}} = (\mathbf{A} \odot \mathbf{B})\mathbf{c}^T + \tilde{\mathbf{z}} \tag{5}$$

where $\tilde{\mathbf{y}} = \mathrm{vec}(\mathbf{Y})$, $\tilde{\mathbf{z}} = \mathrm{vec}(\mathbf{Z})$.

B. Localization Via Radar-Imaging

In the monostatic configuration, $M = N$, $\theta_k = \phi_k$, one possible option is to localize the K targets by beamforming-based radar-imaging techniques [5], [6]. For instance, the classical Capon spectrum is given by

$$\mathrm{P}_{\mathrm{Capon}}(\phi) = \frac{1}{\mathbf{b}^H(\phi)\mathbf{R}_{XX}^{-1}\mathbf{b}(\phi)} \tag{6}$$

where $\mathbf{R}_{XX} \overset{def}{=} (1/L)\mathbf{X}\mathbf{X}^H$ is the sample covariance matrix of the observed snapshots.

Another well-known radar-imaging method is the MUSIC spectral estimator [33], [34]

$$\mathrm{P}_{\mathrm{MUSIC}}(\phi) = \frac{1}{\mathbf{b}^H(\phi)\mathbf{E}_X\mathbf{E}_X^H\mathbf{b}(\phi)} \tag{7}$$

where $\mathbf{E}_X$ is an $N\times(L-K)$ matrix that spans the noise column subspace and can be obtained from the SVD of $\mathbf{X}$.

The targets are then localized by searching for the peaks in the spectrum $\mathrm{P}_{\mathrm{Capon}}(\phi)$ or $\mathrm{P}_{\mathrm{MUSIC}}(\phi)$, which is computed for each DoA of interest.

In the bistatic configuration ($\theta_k \neq \phi_k$), the DoAs can first be estimated in the same way via radar-imaging. Then, provided that $K \leq N$, one can build the estimated receive steering matrix $\hat{\mathbf{B}}$ and finally compute the DoDs by recovering the array-manifold structure on each column of $\hat{\mathbf{A}} = (\hat{\mathbf{B}}^{\dagger}\mathbf{Y})^T$, e.g., with the periodogram-based approach proposed in [35]. Note that the DoDs and DoAs are automatically paired in this hybrid approach. However, in difficult situations where the returned signal has a low power due to high fading or when the targets are closely spaced, it is not always possible to clearly distinguish one peak per target. This yields poor DoAs estimates, and consequently poor DoDs estimates in the second step.

[1]If Doppler is present, the corresponding term can be absorbed by the unknown RCS term—the model remains unchanged, but Doppler cannot be separated from the RCS fluctuations in general.

C. Localization Via 2-D Harmonic Retrieval

When both the transmitter and the receiver employ a uniform linear array, with interelement spacing d_t and d_r, respectively, the data model in (4) becomes

$$y_{n,m} = \sum_{k=1}^{K} \beta_k e^{j(n-1)\mu_k} e^{j(m-1)\psi_k} + z_{n,m} \tag{8}$$

where $\mu_k = (2\pi d_r/\lambda)\sin(\phi_k)$, $\psi_k = (2\pi d_t/\lambda)\sin(\theta_k)$, and λ is the carrier wavelength.

For the ULA configuration, it was shown in [36] that searching for the peaks of $\mathrm{P}_{\mathrm{Capon}}(\phi)$ or $\mathrm{P}_{\mathrm{MUSIC}}(\phi)$ can be accomplished by finding the roots of a polynomial lying close to the unit circle. The resulting root-MUSIC and root-Capon techniques are faster and more accurate than their spectral counterparts [34]. For a generalization of root-MUSIC ideas to arbitrary nonuniform arrays, see [37] and references therein. Finally, given the DoAs estimates, the DoDs can be obtained as explained before, provided that $K \leq N$.

A better approach is to treat (8) for what it really is: a 2-D HR problem, which can be solved by a host of specialized algorithms, including 2-D Unitary ESPRIT [18], 2-D RELAX [38], 2-D multidimensional folding (2-D MDF) [39], 2-D multidimensional embedding—alternating least squares (2-D MDE-ALS) [20], 2-D rank reduction estimator (RARE) [21] or 2-D improved multidimensional folding (2-D IMDF) [23].

D. Uniqueness

For the 2-D HR problem in (8), it was proven in [39] that, if

$$K \leq \left\lceil \frac{N}{2} \right\rceil \left\lceil \frac{M}{2} \right\rceil \tag{9}$$

then the decomposition (8) is almost surely unique, provided that the $2K$ frequencies (μ_k, ψ_k), $k = 1, \ldots, K$, are drawn from a continuous distribution. This bound was relaxed in [23], where it was proven that, if

$$K \leq \max_{\substack{N_1+N_2=N+1 \\ M_1+M_2=M+1}} \min\{2N_1M_1,\ N_2M_2\} \tag{10}$$

where (N_1, N_2) and (M_1, M_2) are arbitrary pairs of positive integers satisfying $N_1+N_2 = N+1$ and $M_1+M_2 = M+1$, respectively, then the decomposition (8) is almost surely unique, given that the $2K$ frequencies $(\mu_k, \psi_k), k = 1, \ldots, K$, are drawn from a continuous distribution. It is important to note that the proofs are constructive—these identifiability bounds are in fact attained by algebraic parameter estimation algorithms. This implies that, unlike the Capon and MUSIC-based estimators described before, the number of targets K can exceed M *and* N when 2-D HR algorithms are used. This is a major advantage of the reformulation of the target localization problem in terms of 2-D HR.

E. Unknown Pulse Waveforms

Suppose that the transmitted waveforms are unknown (e.g., passive radar, which relies on existing "commodity" transmissions) and/or not orthogonal. Equation (3) can be written as

$$\mathbf{X} = \mathbf{B}\tilde{\mathbf{S}}^T + \mathbf{W} \tag{11}$$

where $\tilde{\mathbf{S}} \stackrel{def}{=} \mathbf{S}^T\mathbf{A}\mathbf{\Sigma}$ is unknown and $\mathbf{B}$ is the receive steering matrix. It follows that the DoAs can still be estimated via techniques such as 1-D Capon, 1-D MUSIC or 1-D HR. Instead of exploiting the shift-invariance structure resulting from a single subarray displacement as in standard ESPRIT, one can also exploit the multiple shift-invariance structure of (11) induced by several subarray displacements, which yields a 3-D PARAFAC model [17].

IV. Multiple-Pulses, Bistatic Configuration

A. Data Model

In the previous section, we have considered a CPI consisting of a single pulse period. We now consider a CPI consisting of Q consecutive pulses (configuration 2) and we establish a link between the resulting data model and HR/PARAFAC. Let us assume that the spatial steering matrices $\mathbf{A}$ and $\mathbf{B}$ are constant during the CPI. For a nondispersive propagation medium, the baseband received signal (3) after synchronization can be written on a per-pulse basis as [28]

$$\mathbf{X}_q = \mathbf{B}\mathbf{\Sigma}_q\mathbf{A}^T\mathbf{S} + \mathbf{W}_q, \quad q = 1, \ldots, Q \tag{12}$$

where $\mathbf{X}_q \in \mathbb{C}^{N\times L}$ collects the L samples observed by the N antennas for the qth pulse period, $\mathbf{W}_q$ is the noise-term for the qth pulse period. The diagonal matrix $\mathbf{\Sigma}_q = \mathrm{diag}(\mathbf{c}_q)$ with $\mathbf{c}_q = [\gamma_{1q}, \ldots, \gamma_{Kq}]$ accounts for the Doppler effect and RCS fading. For a Swerling I target model, we have $\gamma_{kq} = \beta_k e^{j(q-1)\chi_k}$, i.e., the RCS coefficients β_k, $k = 1, \ldots, K$, are constant during the CPI, where χ_k is the Doppler frequency of the kth target [28]. For a Swerling II target model, $\gamma_{kq} = \beta_{qk}e^{j(q-1)\chi_k}$, i.e., the RCS coefficients are varying independently from pulse to pulse. Following the same reasoning as in Section III-A, exploitation of the mutual orthogonality of the transmitted waveforms yields the following per-pulse extension of (5)

$$\tilde{\mathbf{y}}_q = (\mathbf{A} \odot \mathbf{B})\mathbf{c}_q^T + \tilde{\mathbf{z}}_q, \quad q = 1, \ldots, Q \tag{13}$$

which can be written in the following compact form:

$$\tilde{\mathbf{Y}} = (\mathbf{A} \odot \mathbf{B})\mathbf{C}^T + \tilde{\mathbf{Z}} \tag{14}$$

where $\tilde{\mathbf{Y}} = [\tilde{\mathbf{y}}_1, \ldots, \tilde{\mathbf{y}}_Q]$, $\tilde{\mathbf{Z}} = [\tilde{\mathbf{z}}_1, \ldots, \tilde{\mathbf{z}}_Q]$ and $\mathbf{C}^T = [\mathbf{c}_1^T, \ldots, \mathbf{c}_Q^T]$. In the following, we denote by $\tilde{\mathcal{Y}}$ and $\tilde{\mathcal{Z}}$ the $N \times M \times Q$ tensors whose matrix representations are $\tilde{\mathbf{Y}}$ and $\tilde{\mathbf{Z}}$, respectively.

B. Localization Via Radar-Imaging

Given (13), one possible strategy is to use the Capon or MUSIC estimators of Section III-B on a per-pulse basis and update the DoAs and DoDs from pulse to pulse. However, if the RCS coefficients are varying from pulse to pulse (Swerling II), the target scintillation phenomenon caused by fading does not allow accurate localization and detection of all targets for every pulse. This is the main motivation for the development of radar-imaging techniques that mitigate RCS fluctuations. For instance, the 2-D Capon spectrum can be written as [7]

$$\mathrm{P}_{\mathrm{Capon}}(\theta, \phi) = \frac{1}{(\mathbf{a}(\theta) \otimes \mathbf{b}(\phi))^H \mathbf{R}_{YY}^{-1}(\mathbf{a}(\theta) \otimes \mathbf{b}(\phi))} \tag{15}$$

where $\mathbf{R}_{YY} = (1/Q)\tilde{\mathbf{Y}}\tilde{\mathbf{Y}}^H$. If the number of targets is known or has been estimated, the MUSIC spectrum can be computed as

$$\mathrm{P}_{\mathrm{MUSIC}}(\theta, \phi) = \frac{1}{(\mathbf{a}(\theta) \otimes \mathbf{b}(\phi))^H \mathbf{E}_Y\mathbf{E}_Y^H(\mathbf{a}(\theta) \otimes \mathbf{b}(\phi))} \tag{16}$$

where $\mathbf{E}_Y$ is the $MN \times (MN - K)$ matrix that contains the noise eigenvectors of $\mathbf{R}_{YY}$, i.e., the eigenvectors associated with the $MN - K$ least significant eigenvalues. The targets are finally localized by searching for the peaks in the 2-D spectrum $\mathrm{P}_{\mathrm{Capon}}(\theta, \phi)$ or $\mathrm{P}_{\mathrm{MUSIC}}(\theta, \phi)$. The latter spectra being computed for every pair of angles of interest, complexity is significant.

C. Localization Via Harmonic Retrieval

When ULAs are employed on the transmitter and the receiver side, using the notation of Section III-C, element $\tilde{y}_{n,m,q}$ of $\tilde{\mathcal{Y}}$ can be written as

$$\tilde{y}_{n,m,q} = \sum_{k=1}^{K} \beta_k e^{j(n-1)\mu_k} e^{j(m-1)\psi_k} e^{j(q-1)\chi_k} + \tilde{z}_{n,m,q} \tag{17}$$

in the Swerling I case. The decomposition in (17) is a 3-D HR problem which can be solved with a variety of specialized algorithms [19], [20], [22], [23]. This yields estimates of the parameters $(\beta_k, \mu_k, \psi_k, \chi_k)$, $k = 1, \ldots, K$, from which the DoAs/DoDs can be extracted. In the Swerling II case, we have

$$\tilde{y}_{n,m,q} = \sum_{k=1}^{K} \beta_{qk} e^{j(n-1)\mu_k} e^{j(m-1)\psi_k} e^{j(q-1)\chi_k} + \tilde{z}_{n,m,q} \tag{18}$$

which is a multiple-snapshots version of the 2-D HR problem that can be solved via the algorithms proposed in, e.g., [19], [24], and [25]. It is also possible to derive a root-version of 2-D Capon and 2-D MUSIC when the transmitter and receiver employ ULAs. The problem then consists of rooting a polynomial of two variables. The resulting optimization problem can be relaxed by sequentially rooting two polynomials, which is the core idea behind the RARE family of algorithms [21], [40].

D. Uniqueness of Harmonic Retrieval

For the 3-D HR problem associated to the Swerling I target model, it was proven in [39], that, if

$$K \leq \left\lceil \frac{N}{2} \right\rceil \left\lceil \frac{M}{2} \right\rceil \left\lceil \frac{Q}{2} \right\rceil \tag{19}$$

then the decomposition (17) is almost surely unique, provided that the $3K$ frequencies (μ_k, ψ_k, χ_k), $k = 1, \ldots, K$, are drawn

from a jointly continuous distribution. Later on, this bound was relaxed in [23], where it was proven that, if

$$K \leq \max_{\substack{N_1+N_2=N+1 \\ M_1+M_2=M+1 \\ Q_1+Q_2=Q+1}} \min\{2N_1M_1Q_1,\ N_2M_2Q_2\} \qquad (20)$$

where (N_1, N_2), (M_1, M_2), and (Q_1, Q_2) are arbitrary pairs of positive integers satisfying $N_1 + N_2 = N + 1$, $M_1 + M_2 = M+1$, and $Q_1+Q_2 = Q+1$, respectively, then the decomposition (17) is almost surely unique, given that the $3K$ frequencies (μ_k, ψ_k, χ_k), $k = 1, \ldots, K$, are drawn from a jointly continuous distribution.

For the multiple-snapshots 2-D HR problem associated to the Swerling II target model, it was proven in [41] that, if

$$\max(M, N) \geq 3 \quad \text{and} \quad K \leq MN - \min(M, N) \qquad (21)$$

then the decomposition (26) is almost-surely unique, provided that the $2K$ frequencies (μ_k, ψ_k), $k = 1, \ldots, K$, are drawn from a jointly continuous distribution and $\mathbf{C} \in \mathbb{C}^{Q\times K}$ is full column rank. If $K > Q$, which occurs when the CPI consists of a very limited number of pulse periods, then $\mathbf{C}$ is not full column rank. In this situation, uniqueness is still covered by a result established in [42], i.e., if

$$K \leq \max_{\substack{N_1+N_2=N+1 \\ M_1+M_2=M+1}} \min\{(N_1-1)(M_1-1),\ 2QN_2M_2\} \qquad (22)$$

then the decomposition (18) is unique, provided that the $2K$ frequencies (μ_k, ψ_k), $k = 1, \ldots, K$, and the entries of $\mathbf{C}$ are drawn from a jointly continuous distribution.

E. Localization Via PARAFAC

From definition 4, it is clear that (14) is the PARAFAC decomposition, written in matrix format, of the noisy observed tensor $\tilde{\mathcal{Y}} \in \mathbb{C}^{N\times M\times Q}$, of which $\tilde{\mathbf{Y}}$ is a matrix representation. Given that the number of targets is known or has been estimated (see Section IV-G), a 3-D PARAFAC model with K components can be fitted to $\tilde{\mathcal{Y}}$ by minimization of the cost function

$$f(\hat{\mathbf{A}}, \hat{\mathbf{B}}, \hat{\mathbf{C}}) = ||\tilde{\mathbf{Y}} - (\hat{\mathbf{A}} \odot \hat{\mathbf{B}})\hat{\mathbf{C}}^T||_F^2 \qquad (23)$$

via various optimization algorithms [43]–[47]. These iterative algorithms do not impose a specific structure on the estimates $\hat{\mathbf{A}}$, $\hat{\mathbf{B}}$ or $\hat{\mathbf{C}}$. The array-manifold structure of $\hat{\mathbf{A}}$ and $\hat{\mathbf{B}}$ is therefore imposed a posteriori (e.g., with the periodogram-based approach [35] in the ULA case), i.e., after convergence. This separation is made possible by the essential uniqueness property of PARAFAC, under mild conditions (see Definition 5 and Section IV-F), i.e., the columns of $\mathbf{A}$ and $\mathbf{B}$ are only subject to scaling and permutation. The latter column-wise permutation is the same for $\mathbf{A}$ and $\mathbf{B}$, so the pairing between DoDs and DoAs is automatic. Since it is not necessary to impose a specific array-manifold structure within the iterative fitting procedure, the PARAFAC framework allows to deal with array geometries more general than ULAs, which is a key advantage over HR algorithms.

In the MIMO radar configuration considered in this section, it is assumed that the steering matrices $\mathbf{A}$ and $\mathbf{B}$ are constant during the CPI. If these matrices are slowly varying from pulse to pulse, one can track the DoAs/DoDs with the adaptive PARAFAC algorithms proposed in [48].

F. Uniqueness of PARAFAC

In the Swerling I ULA configuration, the three loading matrices $\mathbf{A}$, $\mathbf{B}$, and $\mathbf{C}$ have a Vandermonde structure, hence the equivalence to 3-D harmonic retrieval. In the Swerling II ULA configuration, $\mathbf{A}$ and $\mathbf{B}$ are Vandermonde, whereas $\mathbf{C}$ has no specific structure. The uniqueness conditions for the HR problem in Section IV-D can therefore be seen as essential uniqueness conditions for PARAFAC with a Vandermonde structure on two or three loading matrices. If this structure is ignored, essential uniqueness is guaranteed by other sets of conditions. A first result, known as the Kruskal bound [13], states that if

$$\min(M, K) + \min(N, K) + \min(Q, K) \geq 2K + 2 \qquad (24)$$

and the matrices $\mathbf{A}, \mathbf{B}$ and $\mathbf{C}$ are full Kruskal-rank (true if drawn from a jointly continuous distribution), then the PARAFAC decomposition of $\tilde{\mathcal{Y}}$ is essentially unique. In the case where one of the three matrices, say $\mathbf{C}$, is full column rank and the two other matrices, say $\mathbf{A}$ and $\mathbf{B}$, are full rank, it was established in [45], [49] that, if

$$K \geq 2 \quad \text{and} \quad M(M-1)N(N-1) \geq 2K(K-1) \qquad (25)$$

then the PARAFAC decomposition of $\tilde{\mathcal{Y}}$ is essentially unique, almost surely.

G. Estimation of the Number of Targets

Provided that $K \leq \min(MN, Q)$, we can deduce from (14) that $\tilde{\mathbf{Y}}$ is generically rank K, in the noiseless case. It follows that the number of targets can be estimated as the number of significant singular values of $\tilde{\mathbf{Y}}$, i.e., the singular values associated to the signal subspace. If $K > Q$, $\tilde{\mathbf{Y}}$ is not generically rank K. In this situation, the number of targets can still be estimated by the core consistency diagnostic (CORCONDIA) procedure [50].

H. Unknown Pulse Waveforms

The model (14) describes the signals extracted from the matched filterbank, assuming orthogonality and exact knowledge of the transmitted waveforms, and perfect synchronization. If these waveforms are not known or not orthogonal, the matched-filtering operation cannot be performed and one has to work with the raw data

$$\tilde{\mathbf{X}} = (\tilde{\mathbf{S}} \odot \mathbf{B})\mathbf{C}^T + \tilde{\mathbf{W}} \qquad (26)$$

where $\tilde{\mathbf{S}} = \mathbf{S}^T\mathbf{A} \in \mathbb{C}^{L\times K}$ does not have an a priori known structure, $\tilde{\mathbf{X}}$ is the $LN \times Q$ matrix that collects the L samples received by the N antennas for each of the Q pulse periods and $\tilde{\mathbf{W}}$ is the noise term. It follows that (26) is a noisy PARAFAC model. Fitting this model yields estimates of $\mathbf{B}$, $\mathbf{C}$ and $\tilde{\mathbf{S}}$, and the DoAs follow from imposing the array manifold structure onto $\hat{\mathbf{B}}$. In the Swerling I case, $\mathbf{C}$ has a Vandermonde structure and the Doppler frequencies of the targets can thus be extracted after imposing this manifold structure on $\hat{\mathbf{C}}$. In the Swerling II

case, $\mathbf{C}$ has no specific structure and the Doppler frequencies are not identifiable in general.

V. Multiple-Pulses, Multiple Arrays

In this section, we show that the data model for the third configuration can be formulated in terms of the BCD-$(\tilde{N},\ \tilde{M},\cdot)$ of a third-order observed tensor.

A. Data Model

We consider the MIMO radar configuration proposed in [8]:

- $\tilde{M}$ transmit subarrays, with index $m=1,\ldots,\tilde{M}$;
- $\tilde{N}$ receive subarrays, with index $n=1,\ldots,\tilde{N}$;
- mth transmit subarray with M_m closely spaced antennas;
- nth receive subarray with N_n closely spaced antennas;
- $M=\sum_{m=1}^{\tilde{M}} M_m$ is the total number of transmit antennas;
- $N=\sum_{n=1}^{\tilde{N}} N_n$ is the total number of receive antennas;
- the subarrays are sufficiently spaced, so that all transmit and receive subarray pairs experience statistically independent RCS;
- the CPI consists of Q consecutive pulses and the RCS is varying independently from pulse to pulse (Swerling II case);
- K targets in the far field;
- $\mathbf{S}_m=[\mathbf{s}_{m1},\mathbf{s}_{m2},\ldots,\mathbf{s}_{mM_m}]^T\in\mathbb{C}^{M_m\times L}$ holds the M_m narrowband pulse waveforms transmitted by the mth subarray, L being the number of samples per pulse period;
- $\{\theta_{mk}\}_{k=1}^K,\{\phi_{nk}\}_{k=1}^K$ are the DoDs and DoAs with respect to the mth transmit and nth receive array normal, respectively;
- $\mathbf{a}(\theta_{mk})\in\mathbb{C}^{M_m\times 1}$ is the steering vector relative to the mth transmit subarray and kth target, $\mathbf{b}(\phi_{nk})\in\mathbb{C}^{N_n\times 1}$ is the steering vector relative to the nth receive subarray and kth target.

The qth pulse return received by the nth subarray due to the reflection of the waveforms transmitted by the $\tilde{M}$ subarrays can be written, after synchronization, as [8]

$$\mathbf{X}_{nq}=\sum_{k=1}^{K}\mathbf{b}(\phi_{nk})\sum_{m=1}^{\tilde{M}}\beta_{nmqk}\mathbf{a}^T(\theta_{mk})\mathbf{S}_m+\mathbf{W}_{nq} \quad (27)$$

where $\mathbf{X}_{nq}\in\mathbb{C}^{N_n\times L}$ collects the L samples of the signal received by the N_n antennas, $\mathbf{W}_{nq}$ denotes the noise term and β_{nmqk} is the RCS coefficient of the kth target for the (m,n)th subarray pair and qth pulse.

B. Link to Block-Terms Decomposition

We now show that (27) can be seen as a BCD-$(\tilde{N},\ \tilde{M},\cdot)$ of an observed tensor. Let us define the matrices

$$\begin{aligned}
\mathbf{X}_q&=\left[\mathbf{X}_{1q}^T,\mathbf{X}_{2q}^T,\ldots,\mathbf{X}_{\tilde{N}q}^T\right]^T\in\mathbb{C}^{N\times L}\\
\mathbf{W}_q&=\left[\mathbf{W}_{1q}^T,\mathbf{W}_{2q}^T,\ldots,\mathbf{W}_{\tilde{N}q}^T\right]^T\in\mathbb{C}^{N\times L},\\
\mathbf{A}_k&=\mathrm{Diag}\left(\mathbf{a}(\theta_{1k}),\ldots,\mathbf{a}(\theta_{\tilde{M}k})\right)\in\mathbb{C}^{M\times\tilde{M}}\\
\mathbf{B}_k&=\mathrm{Diag}\left(\mathbf{b}(\phi_{1k}),\ldots,\mathbf{b}(\phi_{\tilde{N}k})\right)\in\mathbb{C}^{N\times\tilde{N}}\\
[\mathbf{\Gamma}_{qk}]_{nm}&=\beta_{nmqk},\quad \mathbf{\Gamma}_{qk}\in\mathbb{C}^{\tilde{N}\times\tilde{M}}\\
\mathbf{S}&=\left[\mathbf{S}_1^T,\ldots,\mathbf{S}_{\tilde{M}}^T\right]^T\in\mathbb{C}^{M\times L}.
\end{aligned}$$

Then, (27) can be written as

$$\mathbf{X}_q=\sum_{k=1}^{K}\mathbf{B}_k\mathbf{\Gamma}_{qk}\mathbf{A}_k^T\mathbf{S}+\mathbf{W}_q \quad (28)$$

$q=1,\ldots,Q$. Let us stack the matrices $\mathbf{X}_q$ of (28), $q=1,\ldots,Q$, along the third-dimension to build the $N\times L\times Q$ observed tensor $\mathcal{X}$. We proceed similarly with the matrices $\mathbf{W}_q$ to build $\mathcal{W}\in\mathbb{C}^{N\times L\times Q}$. The Q matrices $\mathbf{\Gamma}_{qk}$, for a fixed index k, are stacked in the $\tilde{N}\times\tilde{M}\times Q$ tensor $\mathcal{G}_k$. Let $\tilde{\mathbf{S}}_k$ be the $L\times\tilde{M}$ matrix defined by

$$\tilde{\mathbf{S}}_k=\mathbf{S}^T\mathbf{A}_k. \quad (29)$$

It follows that (28) can be written in tensor format as

$$\mathcal{X}=\sum_{k=1}^{K}\mathcal{G}_k\bullet_1\mathbf{B}_k\bullet_2\tilde{\mathbf{S}}_k+\mathcal{W}. \quad (30)$$

From definition 7, it is clear that (30) is a BCD in K rank-$(\tilde{N},\ \tilde{M},\cdot)$ terms of the observed tensor $\mathcal{X}$. Thus, the computation of this decomposition yields estimates of the steering matrices $\{\mathbf{B}_k\}_{k=1}^K$, from which the DoAs with respect to all receive subarrays have to be extracted, as will be explained in the sequel.

Let us now assume that all transmitted waveforms are mutually orthogonal such that $(1/L)\mathbf{S}\mathbf{S}^H=\mathbf{I}_M$. After right-multiplication of both sides of (28) by $(1/L)\mathbf{S}^H$, the matched-filtered observed tensor is

$$\mathcal{Y}=\sum_{k=1}^{K}\mathcal{G}_k\bullet_1\mathbf{B}_k\bullet_2\mathbf{A}_k+\mathcal{Z} \quad (31)$$

where $\mathcal{Y}\in\mathbb{C}^{N\times M\times Q}$ and $\mathcal{Z}\in\mathbb{C}^{N\times M\times Q}$ consist of the Q slices $\mathbf{Y}_q=(1/L)\mathbf{X}_q\mathbf{S}^H$ and $\mathbf{Z}_q=(1/L)\mathbf{W}_q\mathbf{S}^H$, respectively.

It is now clear that (31) is a BCD in K rank-$(\tilde{N},\ \tilde{M},\cdot)$ terms of $\mathcal{Y}$, the computation of which yields estimates of $\{\mathbf{B}_k\}_{k=1}^K$ and $\{\mathbf{A}_k\}_{k=1}^K$.

The steering matrices $\mathbf{B}_k\in\mathbb{C}^{N\times\tilde{N}}$ and $\mathbf{A}_k\in\mathbb{C}^{M\times\tilde{M}}$, $k=1,\ldots,K$, of this decomposition have a block-diagonal structure and are full column-rank since we always have $\tilde{N}\leq N$ and $\tilde{M}\leq M$. Moreover, since the RCS coefficients are varying independently from pulse to pulse (Swerling II target model) and since all subarrays are supposed to be sufficiently spaced to experience independent target RCS, it follows that the $\tilde{N}Q\times\tilde{M}$ and $Q\tilde{M}\times\tilde{N}$ matrix representations of $\mathcal{G}_k$, $k=1,\ldots,K$, are generically full column rank for a sufficient number of pulses Q. Hence, the conditions for which the formal definition of the BCD-$(\tilde{N},\ \tilde{M},\cdot)$ applies are satisfied. This decomposition can be computed via an alternating least squares (ALS) algorithm [31], possibly combined with line search to speed up convergence [47] or via the Levenberg-Marquardt algorithm [51].

In the bistatic case $\tilde{M}=\tilde{N}=1$, the BCD-$(\tilde{N},\ \tilde{M},\cdot)$ resumes to PARAFAC, which is consistent with the formulation of the problem in Section IV. In the cases $\{\tilde{M}=1,\ \tilde{N}>1\}$ or $\{\tilde{N}=1,\ \tilde{M}>1\}$, the problem resumes to the computation of the BCD-$(\tilde{N},\ 1,\ \tilde{N})$ or BCD-$(1,\ \tilde{M},\ \tilde{M})$[30], respectively, which are particular cases of the BCD-$(\tilde{N},\ \tilde{M},\cdot)$.

C. Uniqueness

It is clear that in (31), one can arbitrarily permute the K terms. Also, one can postmultiply $\mathbf{B}_k$ by a nonsingular matrix $\mathbf{\Delta}_k \in \mathbb{C}^{\tilde{N}\times\tilde{N}}$ and $\mathbf{A}_k$ by a nonsingular matrix $\mathbf{\Lambda}_k \in \mathbb{C}^{\tilde{M}\times\tilde{M}}$, provided that $\mathcal{G}_k$ is replaced by $\mathcal{G}_k \bullet_1 (\mathbf{\Delta}_k)^{-1} \bullet_2 (\mathbf{\Lambda}_k)^{-1}$. The decomposition is said essentially unique when it is *only* subject to these indeterminacies. Let us define the $(M \times K\tilde{M})$ and $(N \times K\tilde{N})$ matrices $\mathbf{A}$ and $\mathbf{B}$ resulting from the concatenation of the K matrices $\mathbf{A}_k$ and $\mathbf{B}_k$, respectively. It was established in [30] that, if $\operatorname{rank}(\mathbf{A}) = K\tilde{M}$ and $\operatorname{rank}(\mathbf{B}) = K\tilde{N}$, $Q \geq 3$, and if the tensors $\mathcal{G}_k \in \mathbb{C}^{\tilde{N}\times\tilde{M}\times Q}$, $k = 1, \ldots, K$, are generic, i.e., their entries are drawn from jointly continuous probability density functions, then the decomposition of $\mathcal{Y}$ in (31) is essentially unique.

Practically speaking, essential uniqueness is guaranteed if

$$Q \geq 3 \quad \text{and} \quad \min\left(\left\lfloor \frac{M}{\tilde{M}} \right\rfloor, \left\lfloor \frac{N}{\tilde{N}} \right\rfloor\right) \geq K \tag{32}$$

which gives an upper bound on the maximum number of targets that can be identified. Note that this bound is only sufficient. In some cases where this bound is not satisfied, uniqueness can still be guaranteed, but is more difficult to prove [30]. Moreover, this bound has been derived without assuming a specific structure on $\mathbf{A}$ and $\mathbf{B}$. In the application considered in this paper, the latter matrices are very structured since they are block-diagonal and hold array steering vectors on their diagonal. Uniqueness of the BCD-$(\tilde{N},\ \tilde{M}, \cdot)$ with these constraints on $\mathbf{A}$ and $\mathbf{B}$ deserves further research and is left as future work.

D. Final Angle Estimation

Provided that the number of targets K is known or has been estimated, and that essential uniqueness is guaranteed, the computation of the BCD-$(\tilde{N},\ \tilde{M}, \cdot)$ of $\mathcal{Y}$ yields estimates of $\{\mathbf{A}_k\}_{k=1}^K$, $\{\mathbf{B}_k\}_{k=1}^K$, and $\{\mathcal{G}_k\}_{k=1}^K$. However, these estimates are still subject to the aforementioned indeterminacies inherent to the model. In case of perfect estimation, the ith estimate $\hat{\mathbf{A}}_i \in \mathbb{C}^{M\times\tilde{M}}$, $i = 1, \ldots, K$, is equal to one of the true matrices $\mathbf{A}_k$, $k = 1, \ldots, K$[2], up to multiplication by a nonsingular matrix $\mathbf{\Lambda}_k \in \mathbb{C}^{\tilde{M}\times\tilde{M}}$, and similarly for $\hat{\mathbf{B}}_i$

$$\hat{\mathbf{A}}_i = \mathbf{A}_k\mathbf{\Lambda}_k, \quad \hat{\mathbf{B}}_i = \mathbf{B}_k\mathbf{\Delta}_k. \tag{33}$$

In other words, the BCD-$(\tilde{N},\ \tilde{M}, \cdot)$ provides estimates of the column subspaces of the matrices $\mathbf{A}_k$, $\mathbf{B}_k$, but the linear combinations of the subspace vectors that yield the true matrices $\mathbf{A}_k$, $\mathbf{B}_k$, remain unknown in general. In the following, we show that exploitation of the very particular structure of these matrices is sufficient to get unambiguous DoDs/DoAs estimates. The purpose is to recover the block-diagonal structure from the estimates $\{\hat{\mathbf{A}}_i\}_{i=1}^K$, $\{\hat{\mathbf{B}}_i\}_{k=1}^K$, after which the array manifold structure can be imposed.

The $M \times \tilde{M}$ matrices $\hat{\mathbf{A}}_i$ and $\mathbf{A}_k$ can be partitioned as $\hat{\mathbf{A}}_i = [\hat{\mathbf{A}}_{i1}^T, \ldots, \hat{\mathbf{A}}_{i\tilde{M}}^T]^T$ and $\mathbf{A}_k = [\mathbf{A}_{k1}^T, \ldots, \mathbf{A}_{k\tilde{M}}^T]^T$, where $\mathbf{A}_{km} = [\mathbf{0}, \ldots, \mathbf{0}, \mathbf{a}(\theta_{mk}), \mathbf{0}, \ldots, \mathbf{0}] \in \mathbb{C}^{M_m\times\tilde{M}}$, $m = 1, \ldots, \tilde{M}$. From (33), we get

$$\hat{\mathbf{A}}_{im} = [\mathbf{a}(\theta_{mk}), \ldots, \mathbf{a}(\theta_{mk})]\ \operatorname{Diag}([\mathbf{\Lambda}_k]_{m,:}).$$

In other words, in case of perfect estimation, $\hat{\mathbf{A}}_{im}$ is a rank-1 matrix generated by $\mathbf{a}(\theta_{mk})$. It follows that $\mathbf{a}(\theta_{mk})$ can be estimated, up to an irrelevant arbitrary scaling factor, as the left singular vector of $\hat{\mathbf{A}}_{im}$ associated to the largest singular value. The DoD θ_{mk} of the kth target with respect to to the mth transmit subarray is finally estimated after imposing the *a priori* known manifold structure on $\hat{\mathbf{a}}(\theta_{mk})$. The procedure is repeated for all transmit subarrays and all targets. In the ULA case, where the manifold is a spatial harmonic of unknown frequency, this can be accomplished by peak-picking the periodogram of the recovered vector (this is the optimal LS projection onto the manifold in this case). More generally, optimally imposing the manifold structure is a nonlinear regression problem; efficient solution hinges on properly exploiting the array geometry. For arbitrary array geometries but only a single parameter (e.g., DoD), one can resort to 1-D discrete line search, which does not cost much computationally relative to the main part of the overall algorithm. Finally, this procedure is also applied to the $\tilde{N}$ submatrices of $\hat{\mathbf{B}}_i$, for all targets, in order to estimate the DoAs ϕ_{nk}, $n = 1, \ldots, \tilde{N}$, $k = 1, \ldots, K$.

It is interesting to note that (31) can be seen as a set of $\tilde{M}\tilde{N}$ PARAFAC models, due to the block-diagonal structure of $\mathbf{A}_k$ and $\mathbf{B}_k$, $k = 1, \ldots, K$. The $N \times M \times Q$ tensor $\mathcal{Y}$ can be partitioned into a set of $\tilde{M}\tilde{N}$ tensors $\mathcal{Y}_{n,m} \in \mathbb{C}^{N_n\times M_m\times Q}$, where the tensor $\mathcal{Y}_{n,m}$ results from the selection of the elements of $\mathcal{Y}$ associated to the nth receive subarray (subset of N_n rows of $\mathcal{Y}$) and the mth transmit subarray (subset of M_m columns of $\mathcal{Y}$) for the Q pulses. It is not difficult to show that

$$\mathcal{Y}_{n,m} = \sum_{k=1}^{K} \mathbf{b}(\phi_{nk}) \circ \mathbf{a}(\theta_{mk}) \circ [\mathcal{G}_k]_{n,m,:} \tag{34}$$

which is the PARAFAC decomposition in K terms of $\mathcal{Y}_{n,m}$ (see definition 3). Equation (34) is consistent with the results of Section IV, i.e., when a single transmit array and a single receive array are used, the observed tensor obtained after matched-filtering follows a PARAFAC model. Consequently, a PARAFAC decomposition could be computed for all possible pairs of (transmit, receive) subarrays which yields several estimates of all angles. However, since the $\tilde{M}\tilde{N}$ PARAFAC decompositions are computed independently, the DoAs/DoDs estimates will be arbitrarily permuted for each decomposition.

The BCD provides an interesting framework to estimate the DoAs/DoDs with respect to all subarrays, since a single tensor decomposition has to be computed and essential uniqueness of the BCD implies that the pairing between DoAs/DoDs with respect to all subarrays is automatic.

VI. Simulation Results

A. Single Pulse, Bistatic Configuration

In this section, we focus on the first configuration considered in this paper. The mth transmitted waveform, i.e., the

[2]Obviously, the permutation ambiguity is irrelevant in this problem, since the order in which the targets are localized is not important and the pairing of DoDs/DoAs with respect to all subarray pairs is automatic, by definition of essential uniqueness of the decomposition.

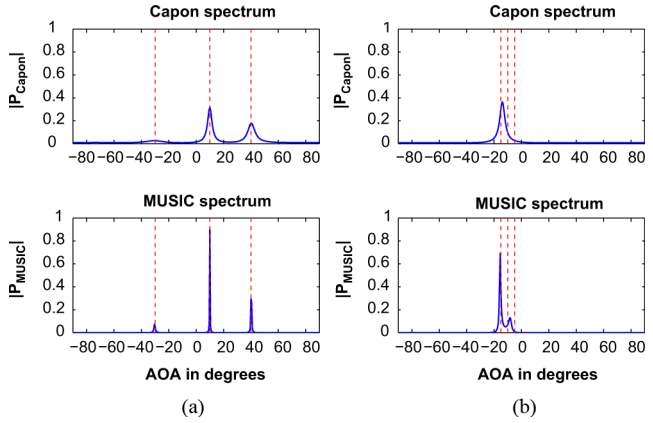

Fig. 3. Typical MUSIC and Capon spectra, for a single pulse realization, monostatic case. Parameters: $M = 6$, $N = 6$, $K = 3$, $L = 512$, SNR $= 10$ dB (a) $(-30^\circ, 10^\circ, 40^\circ)$. (b) $(-5^\circ, -10^\circ, -15^\circ)$.

mth row of $\mathbf{S}$, is generated by $[\mathbf{S}]_{m,:} = (1 + j/\sqrt{2})[\mathbf{H}_L]_{m,:}$, where $\mathbf{H}_L$ is the $L \times L$ Hadamard matrix. We consider ULA transmit and receive arrays with half-wavelength interelement spacing, and a carrier frequency $f_c = 1$ GHz. From (3), the signal-to-noise ratio (SNR) is defined by $\text{SNR} = 10\log_{10}(\|\mathbf{B\Sigma A}^T\mathbf{S}\|_F^2/\|\mathbf{W}\|_F^2)$ dB, where additive white Gaussian noise (AWGN) is assumed. The RCS coefficients (diagonal entries of $\mathbf{\Sigma}$) are randomly drawn from a zero-mean unit-variance Gaussian distribution.

In Fig. 3, we plot typical Capon and MUSIC spectra for $K = 3$ targets, either closely or widely spaced, in the monostatic case, i.e., $\theta_k = \phi_k$, $k = 1, \ldots, K$. These spectra have been computed for all values of θ ranging from -90° to 90°, with an angular step-size of 0.1°. For widely spaced targets, MUSIC and Capon spectra exhibit a peak at each target location, the magnitude of which depends on the power of the signal returned by the target under consideration. For closely spaced targets, it becomes hardly possible to distinguish between three different peaks, which illustrates the limited spatial resolution of radar-imaging methods.

As explained in Section III-C, localization of the multiple targets for a ULA configuration at the transmitter and receiver can be achieved by 2-D HR algorithms. In Fig. 4, we compare the performance of the 2-D MDF [39], 2-D RELAX [38] and 2-D Unitary ESPRIT [18] HR algorithms. For each value of the SNR, we conduct 200 Monte Carlo runs, where the angles are kept fixed and the RCS coefficients are randomly regenerated for each run. The number of samples per pulse is fixed to $L = 512$. The performance criterion is the absolute value of the final angular error, averaged over both angles, all targets and all Monte Carlo runs. The number of targets is fixed to $K = 6$ and we have generated two scenarios: the K targets are either widely spaced or two by two closely spaced. In Fig. 4(a), the number of antennas is $M = N = 5$ and in Fig. 4(b), it is fixed to $M = N = 8$. In the latter case, $K < M$ and $K < N$, so we also plot the performance of the root-MUSIC estimator described in Section III-C. We observe that the performance of all algorithms significantly improve when the number of antennas and the angular spacing between targets increase. In this experiment 2-D Unitary ESPRIT is more accurate than the other algorithms, above a SNR threshold that depends on the number of antennas and angular spacing. For the simulation settings of Fig. 4(b), the average CPU time in seconds per run for each method is: 0.023 for ROOT-MUSIC, 0.021 for 2D-MDF, 0.532 for RELAX-2D, and 0.006 for 2D-UESPRIT. Under the same conditions,the CPU time for the hybrid spectral-MUSIC and spectral-Capon radar-imaging methods described in Section III-B is 1.35 and 1.27, respectively, with angular scanning from -90° to 90° with a step-size of 0.01°.

B. Multiple Pulses, Bistatic Configuration

In this section, we focus on the second MIMO radar configuration, where a CPI consists of Q consecutive pulses. The matrices $\mathbf{S}$, $\mathbf{A}$ and $\mathbf{B}$ are generated as explained in Section VI-A. The SNR is defined by $\text{SNR} = 10\log_{10}(\sum_{q=1}^{Q}\|\mathbf{B\Sigma_q A}^T\mathbf{S}\|_F^2/\sum_{q=1}^{Q}\|\mathbf{W}_q\|_F^2)$ dB, where AWGN is assumed. For the Swerling II target model, each column of $\mathbf{C} \in \mathbb{C}^{Q\times K}$ is generated from a complex Gaussian distribution with zero mean and variance $\sigma_{\beta_k}^2$. For the Swerling I target model, each column of $\mathbf{C}$ is a Vandermonde vector, i.e., $[\mathbf{C}]_{qk} = \beta_k e^{j(q-1)\chi_k}$, where β_k is a sample drawn from a complex Gaussian distribution with zero mean and variance $\sigma_{\beta_k}^2$ and the Doppler frequency χ_k is generated by $\chi_k = (2\pi v_k T_p)/\lambda$, where v_k is the target velocity, $T_p = 5 \cdot 10^{-6}$ is the pulse duration in seconds, and $\lambda = 3 \cdot 10^8/f_c$, with $f_c = 1$ GHz.

In Fig. 5, we have plotted the 2-D MUSIC spectrum $\mathrm{P}(\theta, \phi)$ given by (16), for $K = 5$ targets with DoDs $\{\theta_k\}_{k=1}^K = \{40^\circ, 35^\circ, 30^\circ, -40^\circ, 65^\circ\}$ and DoAs $\{\phi_k\}_{k=1}^K = \{20^\circ, 25^\circ, 30^\circ, 50^\circ, -45^\circ\}$, i.e., for three closely spaced targets and two targets widely spaced from the others. The other parameters are $\{\sigma_k^2\}_{k=1}^K = \{0.3, 0.35, 0.4, 0.45, 0.5\}$, $Q = 50$, $L = 512$ and SNR $= 8$ dB and a Swerling II model is chosen. With $M = 4$ transmit and $N = 4$ receive antennas, 2-D spectral MUSIC does not allow accurate localization of the three closely spaced targets, since one can not clearly distinguish three peaks in the spectra, while the two other targets are well localized. This is an inherent limit to the radar imaging methods, which are very sensitive to the inter-target angular spacing. The spatial resolution significantly improves when the number of antennas increases from $M = N = 4$ to $M = N = 9$—the three closely spaced targets now become distinguishable.

In Fig. 6, a Swerling II model is chosen and we compare the performance of different localization techniques via a Monte Carlo simulation, for $K = 6$ targets that are either widely spaced or two by two closely spaced. The settings are identical to that of the experiment previously conducted in the single-pulse case. Thus, Fig. 6 is the multiple-pulses counterpart of Fig. 4. The RCS coefficients are generated with variances $\{\sigma_k^2\}_{k=1}^K = \{0.3, 0.35, 0.4, 0.45, 0.5, 0.55\}$. For each value of the SNR, 200 Monte Carlo runs have been conducted, the RCS being regenerated for each run while the angles are kept fixed. We have plotted the performance of 2-D spectral Capon and 2-D spectral MUSIC. For the comparison between all methods to be fair, the angular resolution of the two latter techniques is fixed to 0.001°. Since scanning all possible pairs of angles (θ, ϕ) between -90° and 90° with such a small

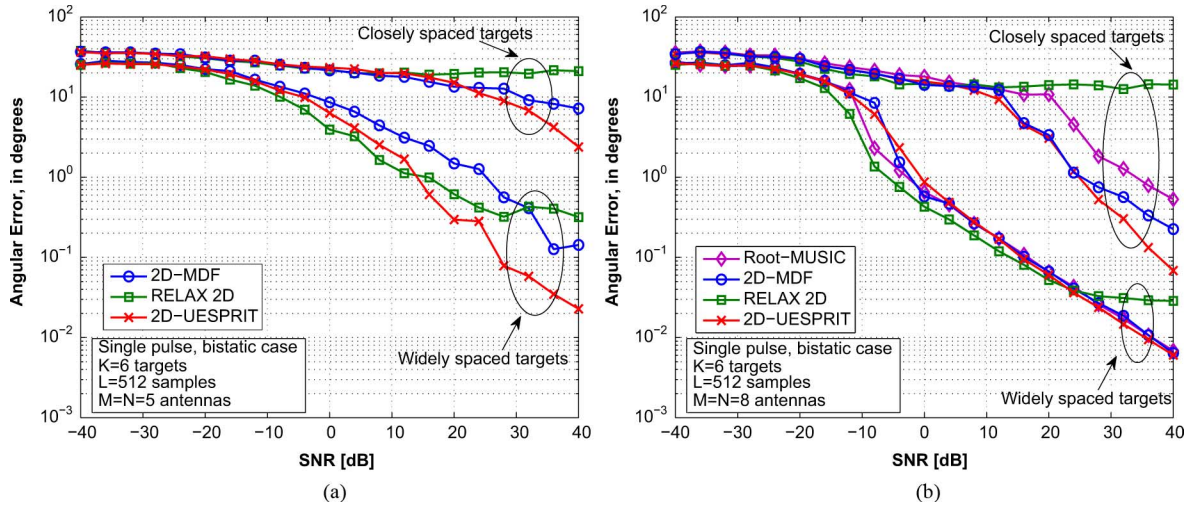

Fig. 4. Single-pulse bistatic configuration. Comparison between 2-D MDF, 2-D RELAX, 2-D Unitary ESPRIT, and 2-D root-MUSIC. $L = 512$ samples. $K = 6$ targets either closely or widely spaced. Widely spaced: $(\theta, \phi) = \{(-80°, 70°), (-60°, 10°), (-40°, 50°), (-20°, -30°), (0°, -10°), (20°, 30°)\}$. Closely spaced: $(\theta, \phi) = \{(-80°, 70°), (-75°, 65°), (-40°, 50°), (-35°, 45°), (0°, -10°), (5°, -15°)\}$. (a) $M = N = 5$ antennas. (b) $M = N = 8$ antennas.

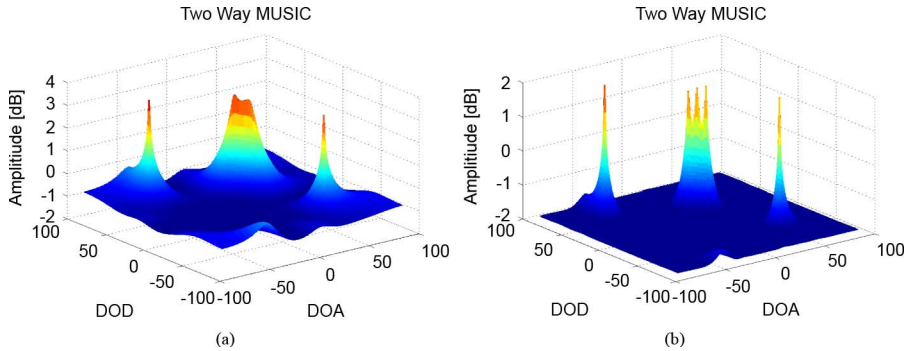

Fig. 5. 2-D MUSIC spectrum for $M = N = 4$ and $M = N = 9$. $K = 5$ targets, $Q = 50$ pulses, $L = 512$ samples, $\mathrm{SNR} = 8$ dB. $\{\theta_k\} = \{40°, 35°, 30°, -40°, 65°\}$, $\{\phi_k\} = \{20°, 25°, 30°, 50°, -45°\}$. (a) $M = N = 4$. (b) $M = N = 9$.

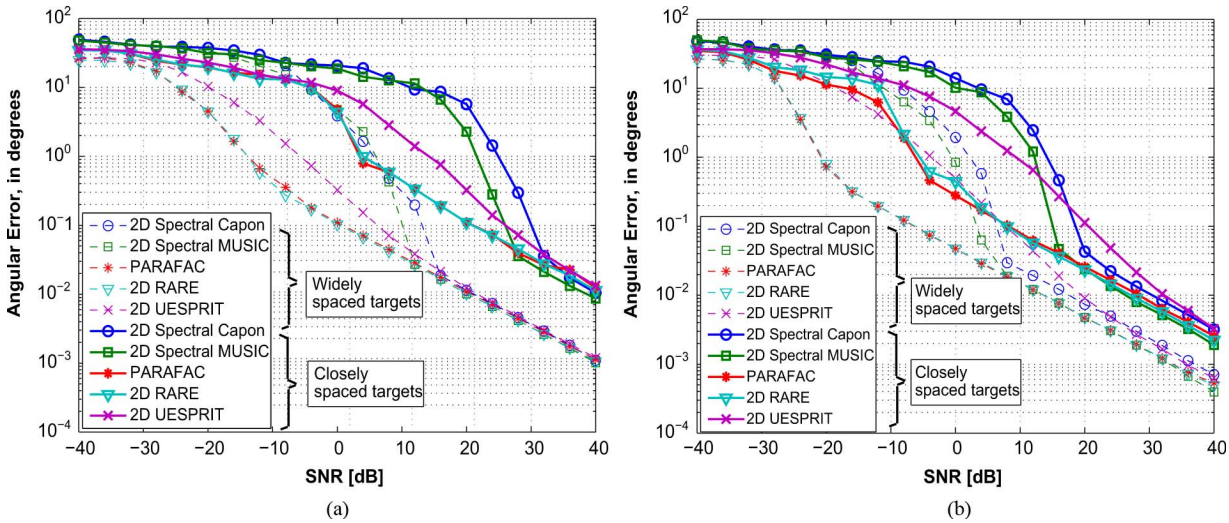

Fig. 6. Swerling II multiple-pulses bistatic configuration. Comparison between 2D Spectral Capon, 2D Spectral MUSIC, PARAFAC, 2D RARE, and 2D Unitary ESPRIT. $Q = 50$ pulses, $L = 512$ samples. $K = 6$ targets either closely or widely spaced. Widely spaced: $(\theta, \phi) = \{(-80°, 70°), (-60°, 10°), (-40°, 50°), (-20°, -30°), (0°, -10°), (20°, 30°)\}$. Closely spaced: $(\theta, \phi) = \{(-80°, 70°), (-75°, 65°), (-40°, 50°), (-35°, 45°), (0°, -10°), (5°, -15°)\}$. (a) $M = N = 5$ antennas. (b) $M = N = 8$ antennas.

angular step-size takes too long, we proceed as follows. The first round of scanning is done with a step-size of 1°, to get a first localization of the four highest peaks of $\mathrm{P}(\theta,\phi)$. Then the estimation is refined individually for each target around those peaks in several rounds, to reach the final resolution of 0.001°. We also plot the performance of the 2-D HR RARE algorithm [21], which generalizes the root-MUSIC ideas to the 2-D case, the performance of 2-D Unitary ESPRIT [18] and the performance of 3-way PARAFAC, where the PARAFAC model (14) is fitted by minimization of the cost function (23) via the algorithm based on Alternating Least Squares combined with Enhanced Line Search (ALS-ELS) [47]. Once the PARAFAC model fitted, the ULA manifold is recovered after convergence with the periodogram-based approach proposed in [35].

From the comparison between Figs. 4 and 6, it is clear that a better angular resolution (regardless of the algorithm used) is achieved when the CPI consists of multiple pulses. For instance, exploitation of this temporal diversity yields a much smaller angular error in difficult scenarios, e.g., when the targets are closely spaced and $K=6$, $M=N=5$. As in the single-pulse scenario, we observe in Fig. 6 that the global performance of all techniques seriously degrade when the targets get closely spaced. From the result of the preliminary experiment (Fig. 5), this was expected for the 2-D spectral Capon and MUSIC techniques. For the algebraic algorithms (PARAFAC, 2-D RARE, 2-D Unitary ESPRIT), closely spaced targets translate to ill-conditioned spatial steering matrices, which makes the separation more difficult. We observe that 3-D PARAFAC and 2-D RARE perform similarly for all scenarios considered in Fig. 6. Above a given SNR threshold, the value of which depends on the number of antennas and the angular spacing between targets, 2-D spectral MUSIC, 2-D spectral Capon and 2-D Unitary ESPRIT reach the performance of the former techniques. For the simulation settings of Fig. 6(b), the average CPU time in seconds per run for each method is: more than 8 for 2D spectral MUSIC and 2D Spectral Capon, 0.51 for PARAFAC, 0.42 for 2D-RARE and 0.03 for 2D-UESPRIT.

From these experiments, we can conclude that 3-D PARAFAC and harmonic retrieval techniques such as 2-D RARE clearly outperform MUSIC-based and Capon-based radar-imaging techniques, since they yield a more accurate localization, especially in difficult scenarios (closely spaced targets, low SNR, small number of antennas), and at a much lower complexity (2-D angular scanning is not needed). As mentioned previously, a key feature of the PARAFAC framework is the possibility to deal with non-ULA arrays since the manifold structure is imposed after convergence, whereas HR algorithms such as 2-D RARE or 2-D ESPRIT, despite a similar or lower complexity than PARAFAC, are designed for ULA configurations only.

In Fig. 7, a Swerling I target model is chosen, and the other parameters are the same as in Fig. 6. The Doppler frequencies are estimated either by the 3-D MDF algorithm [22] or by 3-D Unitary ESPRIT [19]. The performance criterion is the absolute value of the velocity error, averaged over all targets and all Monte Carlo runs. Since the HR algorithms jointly estimate the

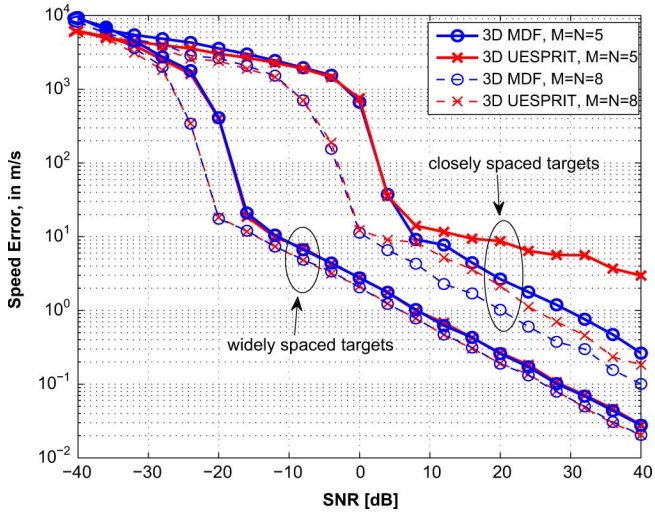

Fig. 7. Swerling I multiple-pulses bistatic configuration. Comparison between 3D Multidimensional Folding algorithm and 3D Unitary ESPRIT algorithm. Same configuration as Fig. 6: $Q=50$ pulses, $L=512$ amples, $K=6$ targets either closely or widely spaced. Velocities: $\{v_k\}_{k=1}^{K}=\{300,250,320,280,150,200\}\,\mathrm{m}\cdot\mathrm{s}^{-1}$.

spatial and temporal parameters, it is expected that the accuracy of the Doppler frequency estimate strongly depends on the inter-angular spacing between the targets. The SNR threshold above which the velocity error becomes "acceptable" depends on the number of antennas and interangular spacing.

C. Multiple Pulses, Multistatic Case

In this section, we focus on the last MIMO radar configuration considered in this paper. In Fig. 8, we illustrate the performance of the estimator based on the BCD-$(\tilde{N},\ \tilde{M},\cdot)$ via a Monte Carlo simulation consisting of 200 runs for each value of the SNR. Q is fixed to 200 pulses, L to 256 samples per pulse and the number of targets to $K=3$. The angles of the K targets with respect to the $\tilde{M}$ transmit and $\tilde{N}$ receive arrays are randomly regenerated for each run, in the interval $[-90°,\ 90°]$, from a uniform distribution and a minimum inter-target spacing of 2° for all subarrays. The RCS coefficients of the K targets are randomly regenerated for each run from a zero-mean unit-variance complex Gaussian distribution. The performance criterion is the absolute value of the angular error, averaged over all transmit and receive angles, over all targets and all Monte Carlo runs.

Fig. 8(a) shows the evolution of the error for the cases $\tilde{N}=\tilde{M}=1$ and $\tilde{N}=\tilde{M}=2$, with either 4 or 6 antennas per subarray. The case $\tilde{N}=\tilde{M}=1$ corresponds to the second MIMO radar configuration, treated in Section IV, and the problem can be solved by PARAFAC. Fig. 8(a) shows that increasing the number of transmit and receive subarrays from 1 to 2 improves the global performance. In Fig. 8(b), the number of antennas is fixed to 4 for all transmit and receive subarrays. The number of transmit subarrays is fixed to $\tilde{M}=3$ and we observe the impact of an increasing number of receive subarrays $\tilde{N}\in\{1,2,3,4\}$ on the global performance.

From these results, it is clear that the spatial diversity resulting from the use of several transmit and receive subarrays

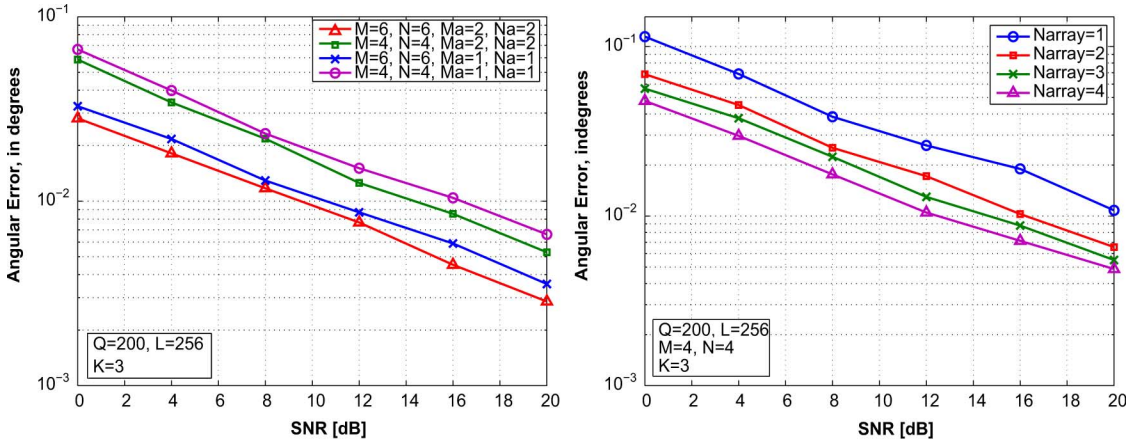

Fig. 8. Monte Carlo simulations, multiple-pulses multistatic configuration. Performance of BCD-$(\tilde{N},\ \tilde{M}, \cdot)$. $K = 3, Q = 200, L = 256$, angles randomly generated with a minimum interangle spacing of 2°. (a) $\tilde{M} = \tilde{N} = \{1, 2\}$ and $M_m = N_n \in \{4, 6\}$. (b) $\tilde{M} = 3, M_m = N_n = 4, \tilde{N} \in \{1, 2, 3, 4\}$.

is exploited by the BCD-$(\tilde{N},\ \tilde{M}, \cdot)$ estimator, which takes the global algebraic structure of the problem into account.

VII. Conclusion

In this paper, we have shown that the multitarget localization problem in various MIMO radar system configurations can be posed and solved as a tensor decomposition or multidimensional HR problem, or hybrids in-between. This viewpoint fully exploits the algebraic structure of the observed data, and diversity in the form of RCS fluctuations commonly viewed as a nuisance. The link between these algebraic methods and the localization problem has been fully fleshed for three different MIMO radar configurations. The rich uniqueness results established for tensor decompositions (with or without Vandermonde structure) yield useful bounds on the number of resolvable targets in this new application area. Numerical experiments illustrated the accuracy and efficacy of the proposed techniques in a variety of pertinent and challenging scenarios, particularly when the targets are closely spaced.

References

[1] D. Nion and N. D. Sidiropoulos, "A PARAFAC-based technique for detection and localization of multiple targets in a MIMO radar system," in *Proc. IEEE Int. Conf. Acoust., Speech Signal Process. (ICASSP)*, 2009.

[2] J. Li and P. Stoica, "MIMO radar with colocated antennas," *IEEE Signal Process. Mag.*, pp. 106–114, Sep. 2007.

[3] A. Haimovich, R. S. Blum, and L. J. Cimini, Jr, "MIMO radar with widely separated antennas," *IEEE Signal Process. Mag.*, pp. 116–129, Jan. 2008.

[4] L. Xu, J. Li, and P. Stoica, "Adaptive techniques for MIMO radar," in *Proc. 4th IEEE Workshop on Sens. Array and Multi Channel Process.*, Waltham, MA, Jul. 2006, pp. 258–262.

[5] L. Xu, J. Li, and P. Stoica, "Radar imaging via adaptive MIMO techniques," in *Proc. 14th Eur. Signal Process. Conf.*, Florence, Italy, Sep. 2006.

[6] J. Li and P. Stoica, *MIMO Radar Signal Processing*. New York: Wiley, 2009.

[7] H. Yan, J. Li, and G. Liao, "Multitarget identification and localization using bistatic MIMO radar systems," *EURASIP J. Adv. in Signal Process.*, vol. 2008, no. ID 283483, 2008.

[8] J. Li, Annu. Rep. Office of Naval Res. Univ. Florida, Gainesville, 2007, MIMO Radar—Diversity Means Superiority.

[9] T. G. Kolda and B. W. Bader, "Tensor decompositions and applications," *SIAM Rev.*, vol. 51, no. 3, pp. 455–500, Sep. 2009.

[10] L. D. Lathauwer, "A survey of tensor methods," in *Proc. ISCAS 2009*, Taipei, Taiwan, 2009, pp. 2773–2776.

[11] R. A. Harshman, "Foundations of the PARAFAC procedure: Model and conditions for an 'explanatory' multi-mode factor analysis," *UCLA Working Papers in Phonet.*, vol. 16, pp. 1–84, 1970.

[12] R. Bro, "Parafac: Tutorial and applications," *Chemom. Intell. Lab. Syst.*, vol. 38, pp. 149–171, 1997.

[13] J. B. Kruskal, "Three-way arrays: Rank and uniqueness of trilinear decompositions, with application to arithmetic complexity and statistics," *Lin. Alg. Appl.*, vol. 18, pp. 95–138, 1977.

[14] N. D. Sidiropoulos and R. Bro, "On the uniqueness of multilinear decomposition of N-way arrays," *J. Chemometr.*, vol. 14, pp. 229–239, 2000.

[15] A. Stegeman and N. D. Sidiropoulos, "On Kruskal's uniqueness condition for the CANDECOMP/PARAFAC decomposition," *Lin. Alg. Appl.*, vol. 420, pp. 540–552, 2007.

[16] A. Smilde, R. Bro, and P. Geladi, *Multi-way Analysis. Applications in the Chemical Sciences*. Chichester, U.K.: Wiley, 2004.

[17] N. D. Sidiropoulos, R. Bro, and G. B. Giannakis, "Parallel factor analysis in sensor array processing," *IEEE Trans. Signal Process.*, vol. 48, pp. 2377–2388, 2000.

[18] M. D. Zoltowski, M. Haardt, and C. P. Mathews, "Closed-form 2D angle estimation with rectangular arrays in element space or beamspace via unitary ESPRIT," *IEEE Trans. Signal Process.*, vol. 44, no. 2, pp. 316–328, Feb. 1996.

[19] M. Haardt and J. Nossek, "Simultaneous schur decomposition of several nonsymmetric matrices to achieve automatic pairing in multidimensional harmonic retrieval problems," *IEEE Trans. Signal Process.*, vol. 46, no. 1, pp. 161–169, 1998.

[20] X. Liu, N. D. Sidiropoulos, and A. Swami, "Blind high-resolution localization and tracking of multiple frequency hopped signals," *IEEE Trans. Signal Process.*, vol. 50, no. 4, pp. 889–901, 2002.

[21] M. Pesavento, C. F. Mecklenbrauker, and J. F. Böhme, "Multidimensional rank reduction estimator for parametric MIMO channel models," *EURASIP J. Appl. Signal Process.*, pp. 1354–1363, Sep. 2004.

[22] K. N. Mokios, N. D. Sidiropoulos, M. Pesavento, and C. E. Mecklenbrauker, "On 3-D harmonic retrieval for wireless channel sounding," *Proc. ICASSP 04*, vol. 2, pp. 89–92, 2004.

[23] J. Liu and X. Liu, "An eigenvector-based approach for multidimensional frequency estimation with improved identifiability," *IEEE Trans. Signal Process.*, vol. 54, no. 12, pp. 4543–4556, Dec. 2006.

[24] J. Liu and X. Liu, "Eigenvector-based n-D frequency estimation from sample covariance matrix," *IEEE Signal Process. Lett.*, vol. 14, no. 3, pp. 209–212, Mar. 2007.

[25] M. Haardt, F. Roemer, and G. D. Gado, "Higher-order SVD-based subspace estimation to improve the parameter estimation accuracy in multidimensional harmonic retrieval problems," *IEEE Trans. Signal Process.*, vol. 56, no. 7, pp. 3198–3213, 2008.

[26] X. Liu, N. D. Sidiropoulos, and T. Jiang, "Multidimensional harmonic retrieval with applications in MIMO wireless channel sounding," in *Space-Time Processing for MIMO Communications*, A. Gershman and N. Sidiropoulos, Eds. New York: Wiley, 2005.

[27] C. E. R. Fernandes, G. Favier, and J. C. M. Mota, "Blind multipath MIMO channel parameter estimation using the PARAFAC decomposition," in *Proc. ICC'2009*, Jun. 2009, pp. 1–5.
[28] C.-Y. Chen and P. P. Vaidyanathan, "MIMO radar space-time adaptive processing using prolate spheroidal wave functions," *IEEE Trans. Signal Process.*, vol. 56, no. 2, pp. 623–635, Feb. 2008.
[29] L. D. Lathauwer, "Decompositions of a higher-order tensor in block terms—Part I: Lemmas for partitioned matrices," *SIAM J. Matrix Anal. Appl.*, vol. 30, no. 3, pp. 1022–1032, 2008.
[30] L. D. Lathauwer, "Decompositions of a higher-order tensor in block terms—Part II: Definitions and uniqueness," *SIAM J. Matrix Anal. Appl.*, vol. 30, no. 3, pp. 1033–1066, 2008.
[31] L. D. Lathauwer and D. Nion, "Decompositions of a higher-order tensor in block terms—Part III: Alternating least squares algorithms," *SIAM J. Matrix Anal. Appl.*, vol. 30, no. 3, pp. 1067–1083, 2008.
[32] C.-Y. Chen and P. P. Vaidyanathan, "A subspace method for MIMO radar space-time adaptive processing," in *Proc. ICASSP 07*, 2007, vol. 2.
[33] R. O. Schmidt, "Multiple emitter location and signal parameter estimation," *IEEE Trans. Antennas Propag.*, vol. 34, pp. 276–280, 1986.
[34] H. L. Van Trees, *Optimum Array Pocessing: Detection, Estimation and Modulation Theory*. New York: Wiley, 2002, pt. IV.
[35] D. C. Rife and R. R. Boorstyn, "Single-tone parameter estimation from discrete-time observations," *IEEE Trans. Inf. Theory*, vol. , IT-20, no. 5, pp. 591–598, Sep. 1974.
[36] A. Barabell, "Improving the resolution performance of eigenstructure-based direction-finding algorithms," in *Proc. ICASSP'83*, Apr. 1983, pp. 336–339.
[37] M. Rübsamen and A. B. Gershman, "Root-MUSIC based direction-of-arrival estimation methods for arbitrary non-uniform arrays," in *Proc. ICASSP'08*, 2008, pp. 2317–2320.
[38] J. Li and P. Stoica, "Efficient mixed-spectrum estimation with applications to target feature extraction," *IEEE Trans. Signal Process.*, vol. 44, no. 2, pp. 281–295, Feb. 1996.
[39] X. Liu and N. D. Sidiropoulos, "Almost sure identifiability of constant modulus multidimensional harmonic retrieval," *IEEE Trans. Signal Process.*, vol. 50, no. 9, pp. 2366–2368, 2002.
[40] M. Pesavento, C. F. Mecklenbrauker, and J. F. Böhme, "Multi-dimensional harmonic estimation using k-D RARE in application to MIMO channel estimation," in *Proc. ICASSP'03*, 2003, vol. 4, pp. 644–647.
[41] T. Jiang, N. D. Sidiropoulos, and J. M. t. Berge, "Almost sure identifiability of multidimensional harmonic retrieval," *IEEE Trans. Signal Process.*, vol. 49, no. 9, pp. 1849–1859, 2001.
[42] J. Liu, X. Liu, and X. Ma, "Multidimensional frequency estimation with finite snapshots in the presence of identical frequencies," *IEEE Trans. Signal Process.*, vol. 55, no. 11, pp. 5179–5194, Nov. 2007.
[43] G. Tomasi and R. Bro, "A comparison of algorithms for fitting the PARAFAC model," *Comp. Stat. Data Anal.*, vol. 50, pp. 1700–1734, 2006.
[44] L. D. Lathauwer, B. D. Moor, and J. Vandewalle, "Computation of the canonical decomposition by means of a simultaneous generalized schur decomposition," *SIAM J. Matrix Anal. Appl.*, vol. 26, no. 2, pp. 295–327, 2004.
[45] L. D. Lathauwer, "A link between the canonical decomposition in multilinear algebra and simultaneous matrix diagonalization," *SIAM J. Matrix Anal. Appl.*, vol. 28, no. 3, pp. 642–666, 2006.
[46] M. Rajih, P. Comon, and R. A. Harshman, "Enhanced line search: A novel method to accelerate PARAFAC," *SIAM J. Matrix Anal. Appl.*, vol. 30, no. 3, pp. 1148–1171, Sep. 2008.
[47] D. Nion and L. D. Lathauwer, "An enhanced line search scheme for complex-valued tensor decompositions. Application in DS-CDMA," *Signal Process.*, vol. 88, no. 3, pp. 749–755, 2008.
[48] D. Nion and N. D. Sidiropoulos, "Adaptive algorithms to track the PARAFAC decomposition of a third-order tensor," *IEEE Trans. Signal Process.*, vol. 57, no. 6, pp. 2299–2310, 2009.
[49] T. Jiang and N. D. Sidiropoulos, "Kruskal's permutation lemma and the identification of CANDECOMP/PARAFAC and bilinear models with constant modulus constraints," *IEEE Trans. Signal Process.*, vol. 52, pp. 2625–2636, 2004.
[50] R. Bro and H. Kiers, "A new efficient method for determining the numbers of components in PARAFAC models," *J. Chemom.*, vol. 17, pp. 274–286, 2003.
[51] D. Nion and L. D. Lathauwer, "A block component model based blind DS-CDMA receiver," *IEEE Trans. Signal Process.*, vol. 56, no. 11, pp. 5567–5579, 2008.

Dimitri Nion was born in Lille, France, on September 6, 1980. He received the electronic engineering degree from ISEN, Lille, in 2003, the M.S. degree from Queen Mary University, London, U.K., in 2003, and the Ph.D. degree in signal processing from the University of Cergy-Pontoise, France, in 2007.

He has been a Postdoctoral Fellow with the Department of Electronic and Computer Engineering, Technical University of Crete, Chania-Crete, Greece (2007-2008) and with the Group Science, Engineering and Technology, K. U. Leuven Campus Kortrijk, Belgium (2008-2010). His research interests include linear and multilinear algebra, blind source separation, signal processing for communications, and adaptive signal processing.

Nicholas D. Sidiropoulos (F'09) received the Diploma degree from the Aristotle University of Thessaloniki, Greece, and the M.S. and Ph.D. degrees from the University of Maryland at College Park (UMCP), in 1988, 1990, and 1992, respectively, all in electrical engineering.

He has been a Postdoctoral Fellow (1994–1995) and Research Scientist (1996–1997) with the Institute for Systems Research, UMCP, and has held positions as Assistant Professor, Department of Electrical Engineering, University of Virginia, Charlottesville (1997–1999), and Associate Professor, Department of Electrical and Computer Engineering, University of Minnesota, Minneapolis (2000–2002). Since 2002, he has been a Professor with the Department of Electronic and Computer Engineering, Technical University of Crete, Chania-Crete, Greece, and Adjunct Professor with the University of Minnesota. His current research interests are primarily in signal processing for communications, convex optimization, cross-layer resource allocation for wireless networks, and multiway analysis.

Prof. Sidiropoulos has served as Distinguished Lecturer (2008-2009) of the IEEE Signal Processing Society (SPS), Chair of the Signal Processing for Communications and Networking Technical Committee (2007-2008), and member of the Sensor Array and Multichannel Processing Technical Committee (2004-2009) of the IEEE SPS. He has also served as an Associate Editor for the IEEE TRANSACTIONS ON SIGNAL PROCESSING (2000-2006) and the IEEE SIGNAL PROCESSING LETTERS (2000-2002). He currently serves on the editorial board of the IEEE SIGNAL PROCESSING MAGAZINE. He received the U.S. NSF/CAREER award in June 1998, and the IEEE SPS Best Paper Award twice (in 2001 and 2007).